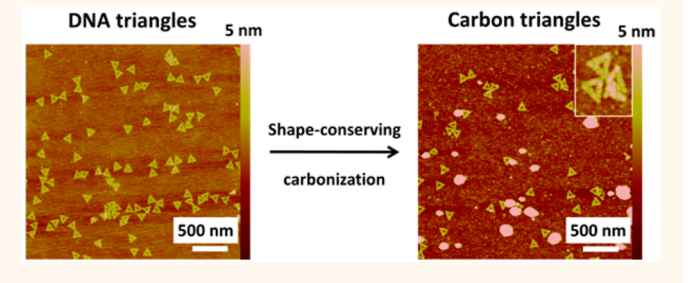


Programmably Shaped Carbon Nanostructure from Shape-Conserving Carbonization of DNA

Feng Zhou, Wei Sun, Karen B. Ricardo, Dong Wang, Eshen, Peng Yin, and Haitao Liu*,

Supporting Information

ABSTRACT: DNA nanostructures are versatile templates for low cost, high resolution nanofabrication. However, due to the limited chemical stability of pure DNA structures, their applications in nanofabrication have long been limited to low temperature processes or solution phase reactions. Here, we demonstrate the use of DNA nanostructure as a template for high temperature, solid-state chemistries. We show that programmably shaped carbon nanostructures can be obtained by a shape-conserving carbonization of DNA nanostructures. The DNA nanostructures were first coated



with a thin film of Al₂O₃ by atomic layer deposition (ALD), after which the DNA nanostructure was carbonized in low pressure H₂ atmosphere at 800-1000 °C. Raman spectroscopy and atomic force microscopy (AFM) data showed that carbon nanostructures were produced and the shape of the DNA nanostructure was preserved. Conductive AFM measurement shows that the carbon nanostructures are electrically conductive.

KEYWORDS: shape-conserving carbonization, DNA nanostructure, high temperature chemistry

ecent advances in DNA nanotechnology make it possible to fabricate arbitrarily shaped 2D and 3D DNA nanostructures through controlled folding and hierarchical assembly of up to several thousands of unique sequenced DNA strands. 1-13 Both individual DNA nanostructures and their assembly can be made with almost arbitrarily shaped patterns at a theoretical resolution down to 2 nm. 11 Furthermore, the deposition of DNA nanostructures on a substrate can be made with precise control of their location and orientation, making them ideal templates for bottom-up nanofabrications. 14-16

As a template, a major limitation of pure DNA nanostructure lies in its limited chemical stability. Hence, almost all reported DNA-based nanofabrications were either based on solution chemistry or conducted at close to room temperature. ^{17–30} For example, solution phase metallization on DNA has been demonstrated using various metals (e.g., Ag, Cu, Ni and Au) and can be made site-specific through modification of DNA nanostructure with binding sites that accept DNA-modified Au or Ag nanoparticles.^{23–27} As another example, Mao and Woolley groups used DNA to pattern vapor-phase deposited metal. ^{28–30} We recently also showed that DNA nanostructure can direct the etching and deposition of SiO2 at room temperature.¹⁷ In all these cases, high quality pattern transfer was achieved; however, due to the low reaction temperature,

the obtained inorganic nanostructures are often of low crystallinity.

High temperature (>500 °C) is often needed for the synthesis and crystallization of most inorganic materials, such as porous carbon. The possibility of using DNA nanostructure to direct chemical synthesis at this extreme temperature range will open up new opportunities in materials design and fabrication. However, DNA decomposes when heated to >250 °C, making it seemingly impossible to achieve pattern transfer from DNA nanostructures under these conditions.

Herein, we demonstrate the fabrication of carbon nanostructures through high temperature (ca. 800 °C) shape-conserving carbonization of DNA nanostructures. With a thin Al₂O₃ film coating, a DNA nanostructure can be converted to carbon nanomaterial while preserving its nanoscale topography. Porous carbon material plays an important role in a wide range of applications, such aerospace structure, thermal management, fluorescent marker, and energy storage. 32-40 The nanoscale structure of porous carbon material is essential to its mechanical, thermal, and electrical properties. For example, nanoscale hierarchical porous structures can be fabricated to show very high strength (modulus ~200 MPa) at low density

Received: August 18, 2015 Accepted: February 4, 2016 Published: February 4, 2016

[†]Department of Chemistry, University of Pittsburgh, Pittsburgh, Pennsylvania 15260, United States

^{*}Wyss Institute for Biologically Inspired Engineering, Harvard University, Boston, Massachusetts 02115, United States

[§]Department of Systems Biology, Harvard Medical School, Boston, Massachusetts 02115, United States

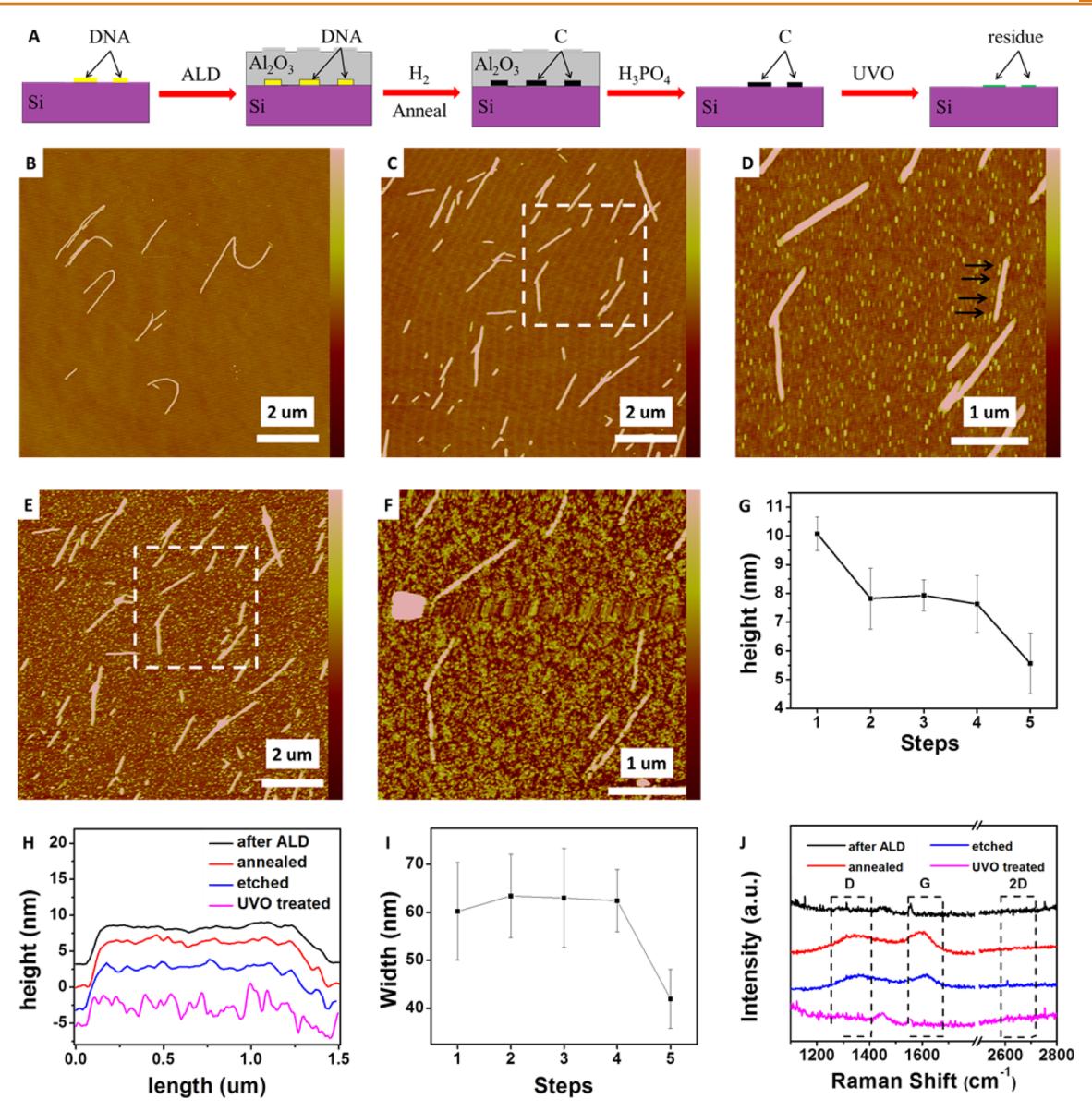


Figure 1. (A) Schematic of shape conserving carbonization of 1D DNA structure and the corresponding AFM topographic images of 1D DNA structure (B) after deposition on top of Si substrate, (C) after ALD of Al_2O_3 film, (D) after annealing at 800 °C for 5 min, (E) after removal of Al_2O_3 film, and (F) after UV/ozone (UVO) treatment. (G) Average height of 1-D DNA at each step. (H) Height profile of the same 1D DNA structure, marked by arrows in panel D. The traces were shifted in the vertical axis for clarity. (I) Average width of 1-D DNA at each step. (J) Raman spectra of samples (C) to (F). The AFM height scale bars for 1D DNA (A-E) are 10 nm. Note: Panels C-F were AFM images taken on the same location; in panels G and I, the horizontal axis represents the five steps of the fabrication process, (1) after deposition on top of Si substrate, (2) after ALD of Al_2O_3 film, (3) after annealing, (4) after removal of Al_2O_3 film and (5) after UV/ozone treatment.

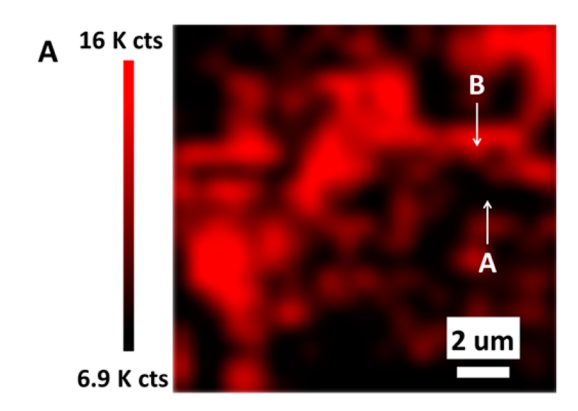
(<100 kg/m³). 41,42 Currently, the porous carbon materials are produced by carbonization of organic/polymer precursors in the presence of an inorganic template. The morphology of existing porous carbon materials is limited to simple periodic lattices. We also note that fabrication of 3D, irregularly shaped carbon nanostructures is extremely challenging using existing approaches. Because DNA nanostructures (1D, 2D, and 3D) can be made into almost arbitrary shapes, our method has the potential to produce arbitrarily shaped 1D, 2D, and 3D carbon nanostructures.

RESULTS

As illustrated in Figure 1A, the carbonization procedure includes four main steps. First, DNA nanostructure was deposited onto a Si wafer substrate. Then, ca. 20 nm of

 Al_2O_3 was conformally coated onto the DNA nanostructure and the Si substrate by atomic layer deposition (ALD). The Al_2O_3 -coated DNA nanostructure was then annealed in a low pressure H_2 atmosphere at high temperature, typically 800–1000 $^{\circ}C$ for 3–5 min. This step converts the DNA to carbon nanostructures. Finally, the Al_2O_3 coating was removed by a H_3PO_4 etch to expose the carbon material for further characterizations. Below, we discuss two examples in more detail.

Shape Conserving Carbonization of 1D DNA Nano-structure: 1D DNA Crystal. The 1D DNA brick crystal was constructed using the DNA brick approach. ⁴⁴ An AFM image of the DNA nanostructure is shown in Figure 1B. The structures are several micrometers in length, 10.1 ± 0.6 nm in height and about 60 ± 10 nm in width (measured from 10



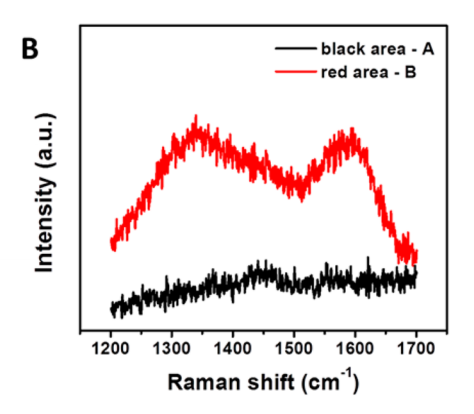


Figure 2. (A) Confocal Raman mapping of annealed 1D DNA structure at 1611 cm⁻¹ and (B) Raman spectra of two spots indicated by the arrows in (A).

different samples). After coating the sample with a ca. 20 nm of Al₂O₃ by ALD, the AFM image of the Al₂O₃ surface still showed the characteristic shape of the DNA nanostructure. This observation is expected because ALD is a conformal coating process; therefore, the topography of the DNA is propagated to the Al₂O₃ surface. We then thermally annealed the Al₂O₃-coated sample at 800 °C for 5 min. The highlighted portion of Figure 1C and D show the same area of the sample before and after the thermal annealing, respectively. Comparing these two images, it is clear that there was no change in the shape and relative position of the nanostructures. This observation is again not surprising given the high melting point of Al₂O₃ (2072 °C). We then proceeded to remove the Al₂O₃ coating by a wet etching of H₃PO₄ to reveal the underlying carbon nanostructures (Figure S1);⁴⁷ we note that this etching is specific to Al₂O₃ and does not attack carbon or SiO₂. In a separate experiment, we also confirmed the removal of Al₂O₃ by X-ray photoelectron spectroscopy (XPS) (Figure S2A and B). After the etching, the sample was again imaged by AFM at the same location and the image is shown in Figure 1E. It can be seen that the overall shape of the nanostructure is identical to that of the DNA template (Figure 1C). Additional experiments demonstrated that these nanostructures are indeed made of carbon (see below).

To quantify the degree of shape conservations, we measured the average height (Figure 1G) of the nanostructures at each stage of the fabrication. A minor decrease of the height was observed after ALD coating (step 1 to step 2) due to the shrinkage of DNA lattice under Al₂O₃ film. Cross sections were measured on a piece of linear DNA crystal, as marked by arrows in Figure 1D, after each processing step. The cross sections showed a high degree of similarity (Figure 1H) showing that the shape of DNA nanostructure is conserved from step 2 to step 4 (i.e., ALD coating, thermal annealing, and removal of Al₂O₃). Finally, Figure 1I shows that there was no change in the width of the nanostructures after carbonization and removal of Al₂O₃.

Micro-Raman spectroscopy was used to characterize the carbon nanomaterial produced by the carbonization procedure. The DNA nanostructure does not produce detectable Raman signal due to its small Raman cross section and low surface coverage. As shown in Figure 1J, the sample became Raman active after thermal annealing. Both D band (1339 cm⁻¹) and G band (1611 cm⁻¹) were observed; both peaks are characteristic of carbon nanomaterials.⁴⁸ The Raman signals persisted after the removal of Al₂O₃ layer, indicating that the Raman active

material was derived from DNA nanostructures underneath the $\mathrm{Al_2O_3}$ film. The presence of G band confirms the formation of $\mathrm{sp^2}$ hybridized carbon materials (i.e., graphitic carbon); the absence of 2D band at ca. 2700 cm⁻¹ indicates the lack of large scale conjugated $\mathrm{sp^2}$ carbon structure. The strong D band indicates the presence of defects in the DNA-derived carbon material; the D band could originate from several sources: presence of edges; formation of $\mathrm{sp^3}$ carbon structure during annealing; and potentially doping by the heteroatoms in DNA (e.g., N atoms, see Figure S2C)). The $\mathrm{sp^2}$ domain size was estimated to be \sim 8.1 nm according to the Tuinstra–Koenig relation (see Supporting Information for detailed calculation). We notice that the $\mathrm{sp^2}$ domain size estimated from the Raman data coincides with the height of the carbon nanostructure.

XPS was also used to further confirm the graphitic nature of the nanostructure product. After carbonization and removal of Al_2O_3 , the C 1s peak of the exposed carbon nanostructures shifted to lower binding energy from that of the as-deposited DNA (Figure S2D and inset). Deconvolution of the C 1s peak identified that the largest contribution in as-deposited DNA sample came from the C–H components (Table S1). After annealing, we observed a significant decrease in nitrogen content and the sp² C=C species increased from 22% to 70%, confirming that the shape-conserving carbonization produced graphitize carbon nanostructures.

To further confirm the formation of carbon nanostructures, we subjected the annealed sample to an UV/ozone treatment after the removal of Al₂O₃. Both D and G bands disappeared (Figure 1J) after the UV/ozone treatment; this observation is consistent with the expected oxidation of carbon material by UV/ozone. Interestingly, the nanostructures were still visible by AFM and there was no change in their shape and relative position (Figure 1F), although their average height and width decreased dramatically (Figure 1G and I). The height profile along an individual DNA crystal structure also showed significant increase of roughness (Figure 1H). These results suggest that although the carbon materials were removed by UV/ozone treatment, certain oxidation-resistant materials were left on the surface. We speculate that these residues are inorganic salt from the buffer or thermal decomposition of DNA.^{21,31}

Finally, to confirm that the Raman activity was due to the annealed DNA nanostructure, we carried out confocal Raman mapping of the annealed 1D DNA crystal sample over a 10 \times 10 μ m area. Figure 2A shows the map of integrated intensity of

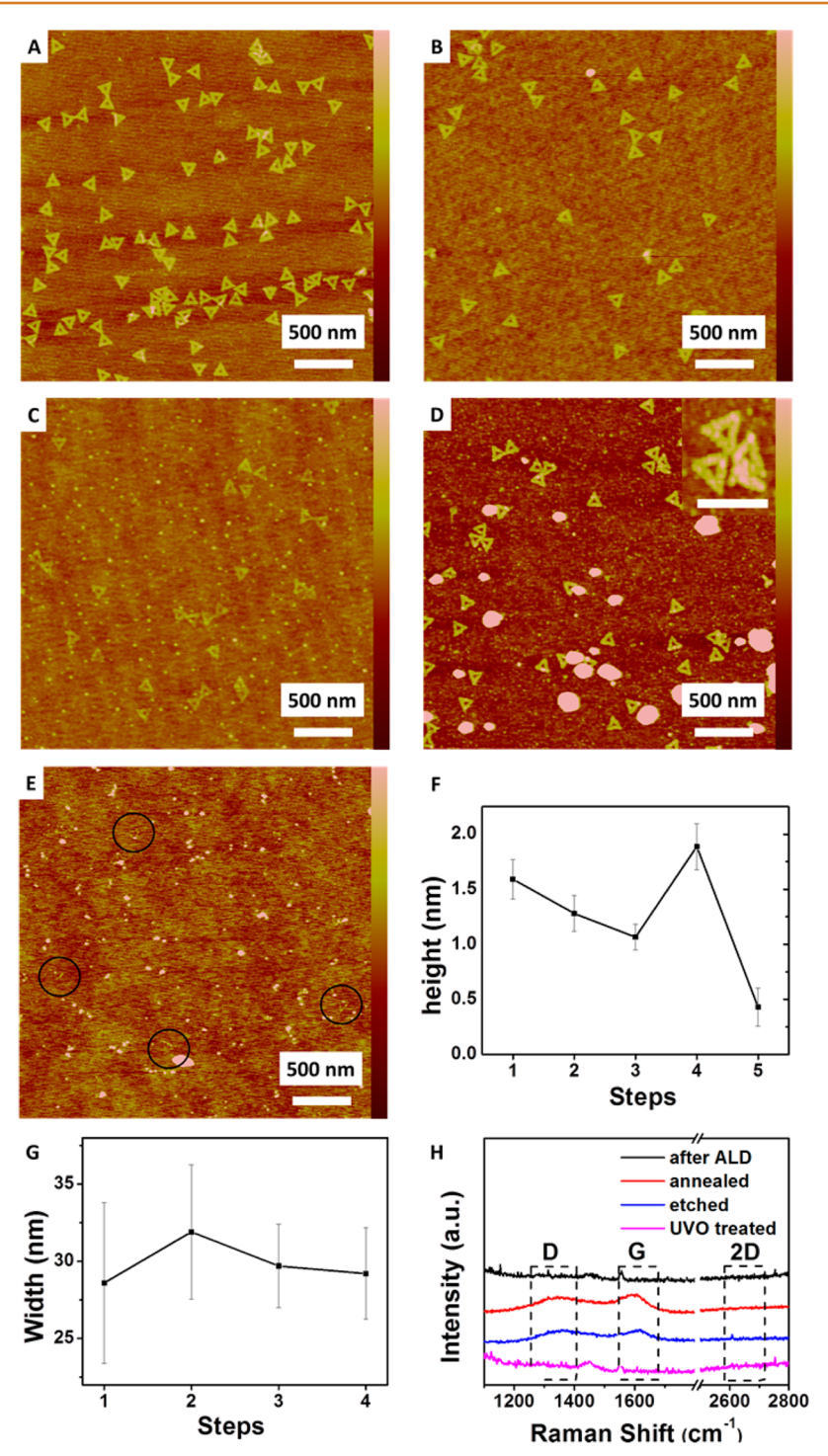


Figure 3. AFM topographic images of DNA triangle (A) after deposition on top of Si substrate, (B) after ALD of Al_2O_3 film, (C) after annealing at 800 °C, (D) after removal of Al_2O_3 film, and (E) after UVO treatment. (F) Average height and (G) width of DNA triangles at each step. (H) Raman spectra of samples (B) to (E). The AFM height scale bars for DNA triangle (A–D) are 5 nm, respectively. The scale bar for the inset of panel D is 200 nm. In panel E, the height bar is 2 nm and the circles highlight several noncarbon residues.

the G peak region (1531 to 1661 cm⁻¹), where linear features of several micrometers in length were clearly observed. Figure 2B shows two representative Raman spectra, one taken from the linear feature and another from a spot nearby that was Raman-inactive. Only the spectrum from the linear structure showed Raman features characteristic of carbon. Those linear structures are consistent with the dimension of the DNA nanostructures measured by AFM (Figure 1A–E), providing

direct evidence that the DNA-to-carbon nanostructure transformation is shape-conserving.

Shape-Conserving Carbonization of 2D-DNA Nanostructure. Following the successful shape-conserving carbonization of the simple linear DNA crystal, efforts were made to extend the methodology to more complex DNA structures. Triangle-shaped DNA nanostructure, with height of 1.6 ± 0.2 nm and width of 28.6 ± 5.2 nm on the edge, was selected for its

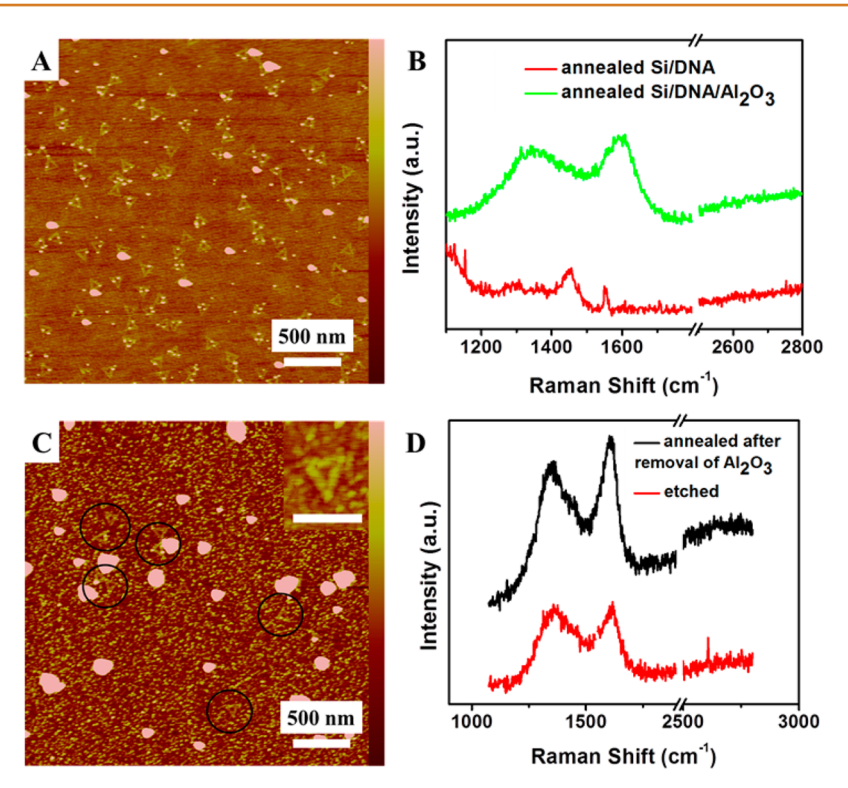


Figure 4. AFM images of (A) the annealed Si/DNA and (C) annealed Si/carbon material; Raman spectra of (B) annealed Si/DNA with and without Al_2O_3 film and (D) comparison of the exposed carbon material before and after the second annealing. The height bars for panels A and C are 5 nm; the scale bar for the inset of panel C is 200 nm. The circles in panel C indicate location of carbon nanostructures.

unique structural features (e.g., linear sides, central void, and sharp tips) as well as its resistance to aggregation. ¹¹ Unlike the 1D DNA crystal, which consists of six overlapping layers of double stranded DNA (ds-DNA), ⁵² the DNA triangle is made of just one layer of ds-DNA. Considering the carbonization yield of sugars at 800 °C is only ca. 30%, ⁵³ we are curious if a continuous carbon nanostructure can be derived from only one layer of ds-DNA.

Similar to the case of 1D DNA crystals, DNA triangles retained their shape after a series of harsh treatments, including ALD, annealing at 800 °C for 5 min and removal of Al₂O₃ by H₃PO₄ etching (Figure 3A-D). The average width of the triangle edges changed less than 4% (Figure 3G), indicating that the DNA nanostructure was well confined during the carbonization procedure. It is interesting to notice that the average height decreased slightly after ALD (from 1.6 ± 0.2 nm to 1.3 \pm 0.2 nm) and annealing (to 1.1 \pm 0.2 nm), but increased (to 1.9 ± 0.2 nm) unexpectedly after the removal of Al₂O₃ (Figure 3F). It is known that the apparent height measured by AFM is sensitive to the tip-substrate interaction and may deviate from the actual height by as much as 1 nm, especially in cases where the sample and the substrate are chemically different (e.g., carbon vs SiO₂).⁵⁴ High resolution AFM image was taken after the removal of Al₂O₃ film; the image presented a continuous, intact triangular nanostructure with a central void (Figure 3D, inset).

Micro-Raman spectroscopy was conducted to detect the presence of carbon materials at each step. Similar to the case of 1D DNA crystal, the DNA triangles sample became Raman active after annealing at high temperature, showing clear D and G bands; such Raman features were still observed after the removal of $\mathrm{Al_2O_3}$ coating (Figure 3H), indicating successful carbonization of DNA material. After exposure to UV/ozone,

the triangle-shaped nanostructure (Figure 3E) disappeared along with the D and G bands in the Raman spectra (Figure 3H), proving that the triangular nanostructures in Figure 3D were indeed made of carbon. In a control experiment, we also treated the samples with UV/ozone before removing the Al_2O_3 coating. In this case, we observed no change in the Raman activity and AFM topography of the sample (Figure S3). This control experiment showed that the carbon material was underneath the Al_2O_3 film and that the Al_2O_3 coating protects the carbon material from oxidation by O_3 .

This shape conserving carbonization approach is compatible with other DNA templates as well. As another example, we show that a large 2D DNA crystal, prepared using the DNA brick approach, amintained its shape after the carbonization. Figure S4A and B are AFM image of the 2D DNA crystal before and after thermal annealing; the height profiles present similar surface features, with the same height of 1.82 ± 0.15 nm. The Raman spectrum shows that D and G bands appeared after annealing (Figure S4E). In addition, Raman mapping showed that the Raman activities originate from micron-sized objects whose dimensions are similar to that of the 2D DNA structures (Figure S4F); this data again shows that the carbonization of DNA nanostructure is a shape-conserving process.

With a thicker 2D DNA crystal of 11.3 ± 0.4 nm in height, we obtained carbonized structures with a height of 7.3 ± 0.7 nm after annealing and removal of Al_2O_3 (Figure S4C). The electrical property of this carbon nanostructure was measured using conductive AFM on the same location of Figure S4C. With an electrical bias of 2 V, the current measured on the carbon nanostructure is 0.28 ± 0.03 nA higher than that of the Si substrate (Figure S4D). Given the fact that the Si substrate is covered by a native oxide layer after the removal of Al_2O_3 (Figure S4D inset), this result indicates that the DNA-derived

carbon nanostructure is conductive to a certain degree. Although only a nanoampere level of current was observed in the conductive AFM measurement, we note that this current may be limited by contact resistance between the AFM tip and the sample; the intrinsic conductivity of the carbon nanostructure may be much higher.

DISCUSSION

Almost any organic materials can be carbonized, including sugar, synthetic polymers, and cellulose.⁴³ Among them, the best substrates for carbonization are those with aromatic rings. DNA is composed of three major components: the phosphate backbone, the sugar, and the four bases. Among the three, sugar is known to carbonize to produce amorphous carbon.⁵³ The four bases are aromatic and structurally similar to a large number of compounds (e.g., polyimide) that carbonize.55 However, bulk DNA decomposes to produce gaseous products when heated to >250 °C,31 making it a challenge to achieve pattern transfer from DNA nanostructure at typical carbonization temperatures (>500 °C). We note that Cu²⁺impregnated DNA filaments have been used to catalyze the growth of graphene nanoribbons; however, the degree of shape conservation was not reported in that work.⁵⁷ Our work is the first to demonstrate precise shape conservation between the DNA templates and the resulting carbon nanostructures.

Systematic Study of Carbonization Condition. We found that the 20 nm Al₂O₃ film is a key component in the success of our experiments. In a control experiment, we annealed a DNA triangle sample without the Al₂O₃ film. Although triangular shaped structures were still observed after annealing (Figure 4A), they are significantly lower (0.58 \pm 0.14 nm) in height, and there was no D and G band observed (Figure 4B, red). We believe that this Raman-inactive structure is the salt residue following decomposition of DNA.^{21,31} In contrast, in the presence of Al₂O₃ film even a single layer of ds-DNA is capable of producing carbon material (Figure 4B, green) and preserving its nanoscale morphology. Our control experiments also showed that a ca. 20 nm of Al₂O₃ coating is impermeable to gas at room temperature (Figure S3). We speculate that in addition to preserving the shape of the nanostructure, Al₂O₃ coating also prevents or slows down the decomposition products of DNA from escaping and as a result increases the carbonization yield.

With the Al_2O_3 coating removed, the carbon nanostructure broke down to small particles after heating at 800 °C for 5 min (Figure 4C), indicating poor stability at high temperature, likely due to the enhanced diffusion. However, storing an annealed sample (with Al_2O_3 removed) at room temperature did not lead to degradation of the nanostructure, as indicated by the AFM images (Figure S5A and B) and Raman spectra (Figure S5C) taken on the same sample. Finally, additional experiments showed that the carbon nanostructures are stable upon repeated AFM imaging and is not affected by laser-induced heating in the time scale of our Raman measurement (see Supporting Information for details).

The annealing conditions were systematically varied to study the effect of temperature, duration and gas environment on the carbonization. To understand the effect of temperature, we carbonized the triangle DNA nanostructure at 780 °C, 800 °C, and 1000 °C; in all three cases, the Raman spectra showed clear D and G bands (Figure S6A), indicating that the carbonization occurred over a wide temperature range. We note that DNA contains sugar and aromatic rings and previous studies have

showed that similar structured materials undergo carbonization at this temperature range.⁵³ To evaluate the effect of annealing time, two Al₂O₃-coated DNA triangle samples were annealed at 800 °C for 5 and 20 min, respectively. Raman spectra (Figure S6B) and AFM images (Figure 3C and S6C) showed that in both cases, the shape conserving carbonization occurred. Additionally, the same 1D DNA crystal sample was annealed at 800 °C for 5 min and then subjected to 1000 °C annealing for another 3 min. AFM topography images (Figure 1D and Figure S6D) and height profiles (Figure S6E) indicate remarkable preservation of nanostructure and Raman spectra (Figure S6F) show D and G peaks after both annealing. These results show that the carbonization was completed within 5 min and the carbon structure can be preserved at high temperature during extended heat treatment, owing to the high melting point of Al₂O₃ film. The effect of gas environment was studied by heating the Al₂O₃/DNA/Si samples in H₂, Ar, and air at 800 °C for 5 min. In the case of H₂ and Ar, the Raman spectra showed clear D and G peaks, whereas no graphitic signal was observed from the samples annealed in air (Figure S6G). Furthermore, for the sample annealed in H2, we subjected it to a second annealing in air at 800 °C for another 5 min, and the D and G peaks vanished (Figure S6H). Compared with the previous demonstration of additional annealing in H2 atmosphere, the results indicate that the carbonization procedure required inert atmosphere since the Al₂O₃ film was not impermeable to O2 at high temperature although it does provide protection against UV/O₃ oxidation (Figure S3).

Origin of Carbon. Carbon source other than DNA nanostructure could be introduced during the carbonization process. Possible non-DNA carbon source include the airborne carbon contamination, ⁵⁸ the byproduct of ALD, ⁵⁹ and the buffer solution used for DNA deposition. Control experiments were conducted to determine the possible contribution from all these sources, as detailed below.

As shown in Figure S7A, the Raman spectrum taken from annealed Al₂O₃/Si, which was prepared from direct deposition of Al₂O₃ on the blank Si surface (without DNA), showed no D or G peak, indicating the ALD product residue and airborne carbon contaminations do not produce carbon material. Similarly, we found that the buffer solution did not introduce significantly amount of carbon precursor. During the deposition of the 1D DNA crystals, the Si wafer was rinsed with water after the DNA deposition. A control sample was prepared by soaking a Si wafer in a DNA-free buffer solution, followed by rinsing the wafer with water. This sample was then coated with Al₂O₃ and no carbon material was detected by Raman spectroscopy after thermal annealing (Figure S7A). The preparation for DNA triangle and 2D DNA crystal samples involve rinsing with an ethanol-water mixture. In this case, the control sample (Si wafer soaked in DNA-buffer then rinsed with ethanol-water mixture) showed weak D and G peaks in the Raman spectrum after ALD coating and annealing (Figure S7A). However, the Raman signal intensity is 22%-27% of that from samples having deposited 1D and 2D DNA crystals.

CONCLUSIONS

We have demonstrated that DNA nanostructures can be converted to carbon nanostructures of the same shape by high temperature annealing. A thin Al_2O_3 coating was found to be essential to preserving the shape of the carbon nanostructures. Although the application of DNA nanostructures have long been limited to room temperature, aqueous environments, our

work showed that they are also useful as material templates for high temperature solid state chemistries. We hope that this case study may catalyze further use of DNA nanostructure in the fabrication of inorganic nanostructures.

METHODS

1.1. Preparation of DNA Nanostructure on Si Substrate. *Preparation of DNA Nanostructure.* Synthetic and M13mp18 DNA for preparing the DNA triangle origami were purchased from IDT and New England Biolabs, respectively. 2D DNA triangles was prepared using DNA origami approach.¹¹ 1D-DNA crystals and 2D DNA crystals were prepared using the DNA brick approach.⁵²

Deposition of DNA Nanostructure on Si Wafer. Silicon wafers were purchased from University Wafers. It was cleaned with hot piranha solution (7:3 (v/v) of concentrated H_2SO_4 :35% H_2O_2). Warning: Piranha solution presents an explosion danger and should be handled with extreme care; it is a strong oxidant and reacts violently with organic materials. All work should be performed in a fume hood. Wear proper protective equipment. Triangular DNA origami and 2D DNA crystals were assembled on the substrate by incubating 2 μ L of DNA solution on the substrate in a wet chamber for 40 min before blowing away the solution. The substrate was immersed in a 9/1 (v/v) ethanol/water solution to remove the salt from the buffer solution. 1D-DNA was assembled by incubating 2 μ L of DNA solution on the substrate for 4 min and then washing the substrate with 400 μ L of deionized water. After the deposition of DNA, the substrate was preceded to the ALD step within 1 day.

- **1.2. Deposition of Protective Inorganic Film.** Atomic layer deposition (ALD) of Al_2O_3 on DNA/Si substrate: The ALD was conducted using a Cambridge Nanotech Fiji ALD system by Dr. Kline and Dr. Bowman in ECE department at Carnegie Mellon University. We used trimethylaluminum (TMA) and H_2O as precursor. The chamber and substrate heaters were set to 200 °C and the throttle valve position was set to give 200 mTorr at 260 sccm total Ar flow. The deposition looped 200 times of 0.006 s TMA pulse, 10 s interval, 0.06 s H_2O pulse and 10 s interval. The preset deposition thickness of oxide film was 20 nm and the experimental thickness of the film was measured by ellipsometry. The surface of the sample was imaged using tapping mode AFM.
- **1.3. Annealing Experiment.** Typically, the prepared sandwich-like substrate was placed at the center of a quartz plate in a 1 in. diameter fused quartz tube. The furnace tube was evacuated and H_2 gas flowed at a rate of 2.0 standard cubic centimeters per minute (sccm) with a pressure of 70 mTorr for 5 min. Then the furnace was heated to 800 °C under a 2.0 sccm of H_2 . Time was recorded when the temperature reach the setting value. Then the substrate was cooled to room temperature under H_2 gas flow and taken out from the tube furnace.
- **1.4. Etching Experiment.** The Al_2O_3 film was etched in the 4.56 M H_3PO_4 solution for 1 h, followed by rinsing with 1 M H_3PO_4 and H_2O . As shown in Figure S1, the etching procedure was studied on the annealed Al_2O_3/SiO_2 wafer and the etching rate is about 0.3 nm/sec.
- **1.5. UV/Ozone Experiment.** The substrate was subjected in the Novascan PSD Pro Series UV/ozone cleaner for UVO treatment. The UV/O_3 chamber was flushed with oxygen for 5 min before UV irradiation. The typical duration for the treatment was 60 min.
- **1.6. Characterization Methods.** Raman Spectroscopy. Individual Raman spectra were collected using a custom-built Raman setup consisting of a Nikon inverted microscope (Nikon Eclipse Ti/U with a 40× objective, NA: 0.60), a long pass edge filter (Semrock), a single stage spectrograph (Andor Shamrock 303), and an back illuminated CCD camera (Andor iDus). Each spectrum was taken with 20 to 600 s integration time under a low incident laser power of 1.2–1.4 mW, thus the heating effects can be neglected.

Confocal Raman Mapping. The confocal Raman mapping was performed using a Renishaw inVia Raman microscope, with 633 nm laser excitation. The spatial step was 0.5 μ m, and the integration time for each spot was 10 s. The laser power was 1.7 mW and the grating was 1800 L/mm.

Atomic Force Microscopy. Surface morphology was measured using tapping mode atomic force microscopy (AFM) using a Veeco Dimension 3100 or an Asylum Research MFP-3D with μ masch NSC15 tips in air. Contact mode and conductive AFM images were taken on an Asylum Research MFP-3D AFM using an ORCA module and BudgetSensors Tap300E-G tips in air.

Ellipsometry. Thickness measurements of the oxide film were carried out on an alpha-SE Ellipsometer. The literature refractive index values of SiO₂ and Al₂O₃ were 1.450 and 1.921, respectively. The refractive index was also measured by using Cauchy self-fitting model.

X-ray Photoelectron Spectroscopy (XPS). XPS was conducted in the Escalab 250XI XPS microscope. Deconvolution of the C 1s peak was calculated using XPSPEAK 4.1. We note that the carbon XPS data should be interpreted with caution because airborne hydrocarbon could contaminate the surface. This contamination is known to occur on SiO_2 surface; we recently also reported that the contamination occurs on graphitic surface as well.⁵⁸

ASSOCIATED CONTENT

S Supporting Information

The Supporting Information is available free of charge on the ACS Publications website at DOI: 10.1021/acsnano.5b05159.

Additional discussion, etching rate, XPS analysis, AFM images, cross-sectional images, Raman spectra, relative areas. (PDF)

AUTHOR INFORMATION

Corresponding Author

*E-mail: hliu@pitt.edu.

Author Contributions

H.L. designed and directed the experiments. F.Z., W.S., J.S., D.W., and K.R. conducted the experiments. All authors discussed the results. H.L. and F.Z. cowrote the manuscript with input from all authors.

Notes

The authors declare no competing financial interest.

ACKNOWLEDGMENTS

H.L. acknowledges partial support from AFOSR (YIP grant FA9950-13-1-0083), ONR (N000141310575 and N00014151252), NSF (CHE-1507629), the Mascaro Center for Sustainable Innovation, and the Central Research Development Fund of the University of Pittsburgh. P.Y. acknowledges funding support from NSF (CMMI-1333215 and CMMI-1344915), ONR (N00014-14-1-0610), and AFOSR (MURI, FA9550-15-1-0514).

REFERENCES

- (1) Zhang, H. L.; Chao, J.; Pan, D.; Liu, H. J.; Huang, Q.; Fan, C. H. Folding Super-Sized DNA Origami with Scaffold Strands from Long-Range PCR. *Chem. Commun.* **2012**, *48*, 6405–6407.
- (2) Wei, B.; Dai, M. J.; Yin, P. Complex Shapes Self-Assembled from Single-Stranded DNA Tiles. *Nature* **2012**, *485*, *623*.
- (3) Zhao, Z.; Liu, Y.; Yan, H. Organizing DNA Origami Tiles Into Larger Structures Using Preformed Scaffold Frames. *Nano Lett.* **2011**, 11, 2997–3002.
- (4) Woo, S.; Rothemund, P. W. K. Programmable Molecular Recognition Based on the Geometry of DNA Nanostructures. *Nat. Chem.* **2011**, *3*, 620–627.
- (5) Endo, M.; Sugita, T.; Rajendran, A.; Katsuda, Y.; Emura, T.; Hidaka, K.; Sugiyama, H. Two-Dimensional DNA Origami Assemblies Using a Four-Way Connector. *Chem. Commun.* **2011**, *47*, 3213–3215.
- (6) Castro, C. E.; Kilchherr, F.; Kim, D. N.; Shiao, E. L.; Wauer, T.; Wortmann, P.; Bathe, M.; Dietz, H. A Primer to Scaffolded DNA Origami. *Nat. Methods* **2011**, *8*, 221–229.

(7) Seeman, N. C. Nanomaterials Based on DNA. Annu. Rev. Biochem. 2010, 79, 65–87.

- (8) Douglas, S. M.; Dietz, H.; Liedl, T.; Hogberg, B.; Graf, F.; Shih, W. M. Self-Assembly of DNA Into Nanoscale Three-Dimensional Shapes. *Nature* **2009**, *459*, 414–418.
- (9) Dietz, H.; Douglas, S. M.; Shih, W. M. Folding DNA Into Twisted and Curved Nanoscale Shapes. *Science* **2009**, 325, 725–730.
- (10) Seeman, N. C. An Overview of Structural DNA Nanotechnology. *Mol. Biotechnol.* **2007**, *37*, 246–257.
- (11) Rothemund, P. W. K. Folding DNA to Create Nanoscale Shapes and Patterns. *Nature* **2006**, 440, 297–302.
- (12) Liu, W. Y.; Zhong, H.; Wang, R. S.; Seeman, N. C. Crystalline Two-Dimensional DNA-Origami Arrays. *Angew. Chem., Int. Ed.* **2011**, 50, 264–267.
- (13) Han, D. R.; Pal, S.; Nangreave, J.; Deng, Z. T.; Liu, Y.; Yan, H. DNA Origami with Complex Curvatures in Three-Dimensional Space. *Science* **2011**, 332, 342–346.
- (14) Hung, A. M.; Noh, H.; Cha, J. N. Recent Advances in DNA-Based Directed Assembly on Surfaces. *Nanoscale* **2010**, *2*, 2530–2537.
- (15) Gerdon, A. E.; Oh, S. S.; Hsieh, K.; Ke, Y.; Yan, H.; Soh, H. T. Controlled Delivery of DNA Origami on Patterned Surfaces. *Small* **2009**, *5*, 1942–1946.
- (16) Kershner, R. J.; Bozano, L. D.; Micheel, C. M.; Hung, A. M.; Fornof, A. R.; Cha, J. N.; Rettner, C. T.; Bersani, M.; Frommer, J.; Rothemund, P. W. K.; Wallraff, G. M. Placement and Orientation of Individual DNA Shapes on Lithographically Patterned Surfaces. *Nat. Nanotechnol.* **2009**, *4*, 557–561.
- (17) Surwade, S. P.; Zhou, F.; Wei, B.; Sun, W.; Powell, A.; O'Donnell, C.; Yin, P.; Liu, H. Nanoscale Growth and Patterning of Inorganic Oxides Using DNA Nanostructure Templates. *J. Am. Chem. Soc.* **2013**, *135*, 6778–6781.
- (18) Zhang, G.; Surwade, S. P.; Zhou, F.; Liu, H. DNA Nanostructure Meets Nanofabrication. *Chem. Soc. Rev.* **2013**, 42, 2488–2496.
- (19) He, Y.; Liu, H.; Chen, Y.; Tian, Y.; Deng, Z.; Ko, S. H.; Ye, T.; Mao, C. DNA-Based Nanofabrications. *Microsc. Res. Tech.* **2007**, *70*, 522–529.
- (20) Surwade, S. P.; Zhao, S.; Liu, H. Molecular Lithography through DNA-Mediated Etching and Masking of SiO₂. *J. Am. Chem. Soc.* **2011**, 133, 11868–11871.
- (21) Zhou, F.; Michael, B.; Surwade, S. P.; Ricardo, K. B.; Zhao, S.; Liu, H. Mechanistic Study of the Nanoscale Negative-Tone Pattern Transfer from DNA Nanostructures to SiO₂. *Chem. Mater.* **2015**, 27, 1692–1698.
- (22) Schreiber, R.; Kempter, S.; Holler, S.; Schüller, V.; Schiffels, D.; Simmel, S. S.; Nickels, P. C.; Liedl, T. DNA Origami-Templated Growth of Arbitrarily Shaped Metal Nanoparticles. *Small* **2011**, 7, 1795–1799.
- (23) Braun, E.; Eichen, Y.; Sivan, U.; Ben-Yoseph, G. DNA-Templated Assembly and Electrode Attachment of a Conducting Silver Wire. *Nature* **1998**, *391*, 775–778.
- (24) Becerril, H. A.; Woolley, A. T. DNA-Templated Nanofabrication. *Chem. Soc. Rev.* **2009**, *38*, 329–337.
- (25) Pilo-Pais, M.; Goldberg, S.; Samano, E.; LaBean, T. H.; Finkelstein, G. Connecting the Nanodots: Programmable Nanofabrication of Fused Metal Shapes on DNA Templates. *Nano Lett.* **2011**, *11*, 3489–3492.
- (26) Pearson, A. C.; Liu, J.; Pound, E.; Uprety, B.; Woolley, A. T.; Davis, R. C.; Harb, J. N. DNA Origami Metallized Site Specifically to Form Electrically Conductive Nanowires. *J. Phys. Chem. B* **2012**, *116*, 10551–10560.
- (27) Liu, J.; Geng, Y.; Pound, E.; Gyawali, S.; Ashton, J. R.; Hickey, J.; Woolley, A. T.; Harb, J. N. Metallization of Branched DNA Origami for Nanoelectronic Circuit Fabrication. *ACS Nano* **2011**, *5*, 2240–2247
- (28) Becerril, H. A.; Woolley, A. T. DNA Shadow Nanolithography. *Small* **2007**, *3*, 1534–1538.

(29) He, Y.; Ye, T.; Ribbe, A. E.; Mao, C. DNA-Templated Fabrication of Two-Dimensional Metallic Nanostructures by Thermal Evaporation Coating. *J. Am. Chem. Soc.* **2011**, *133*, 1742–1744.

- (30) Deng, Z.; Mao, C. Molecular Lithography with DNA Nanostructures. *Angew. Chem., Int. Ed.* **2004**, 43, 4068–4070.
- (31) Kim, H.; Surwade, S. P.; Powell, A.; O'Donnell, C.; Liu, H. Stability of DNA Origami Nanostructure Under Diverse Chemical Environments. *Chem. Mater.* **2014**, *26*, 5265–5273.
- (32) Nakao, H.; Tokonami, S.; Yamamoto, Y.; Shiigi, H.; Takeda, Y. Fluorescent Carbon Nanowires Made by Pyrolysis of DNA Nanofibers and Plasmon-Assisted Emission Enhancement of Their Fluorescence. *Chem. Commun.* **2014**, *50*, 11887–11890.
- (33) Gui, X. C.; Wei, J. Q.; Wang, K. L.; Cao, A. Y.; Zhu, H. W.; Jia, Y.; Shu, Q. K.; Wu, D. H. Carbon Nanotube Sponges. *Adv. Mater.* **2010**, 22, 617–621.
- (34) Frackowiak, E.; Beguin, F. Carbon Materials for the Electrochemical Storage of Energy in Capacitors. *Carbon* **2001**, *39*, 937–950.
- (35) Gallego, N. C.; Klett, J. W. Carbon Foams for Thermal Management. *Carbon* **2003**, *41*, 1461–1466.
- (36) Klett, J.; Hardy, R.; Romine, E.; Walls, C.; Burchell, T. High-Thermal-Conductivity, Mesophase-Pitch-Derived Carbon Foams: Effect of Precursor on Structure and Properties. *Carbon* **2000**, *38*, 953–973.
- (37) Zhang, L. L.; Zhao, X. S. Carbon-Based Materials as Supercapacitor Electrodes. *Chem. Soc. Rev.* **2009**, 38, 2520–2531.
- (38) Balandin, A. A. Thermal Properties of Graphene and Nanostructured Carbon Materials. *Nat. Mater.* **2011**, *10*, 569–581.
- (39) Zheng, J.; Birktoft, J. J.; Chen, Y.; Wang, T.; Sha, R.; Constantinou, P. E.; Ginell, S. L.; Mao, C.; Seeman, N. C. From Molecular to Macroscopic *Via* the Rational Design of a Self-Assembled 3d DNA Crystal. *Nature* **2009**, *461*, 74–77.
- (40) Chesnokov, S. A.; Nalimova, V. A.; Rinzler, A. G.; Smalley, R. E.; Fischer, J. E. Mechanical Energy Storage in Carbon Nanotube Springs. *Phys. Rev. Lett.* **1999**, *82*, 343–346.
- (41) Cheung, K. C.; Gershenfeld, N. Reversibly Assembled Cellular Composite Materials. *Science* **2013**, *341*, 1219–1221.
- (42) Meza, L. R.; Das, S.; Greer, J. R. Strong, Lightweight, and Recoverable Three-Dimensional Ceramic Nanolattices. *Science* **2014**, 345, 1322–1326.
- (43) Sazanov, Y. N.; Gribanov, A. V. Criteria of Polymer Carbonization. Russ. J. Appl. Chem. 2009, 82, 473–482.
- (44) Lee, J.; Kim, J.; Hyeon, T. Recent Progress in the Synthesis of Porous Carbon Materials. *Adv. Mater.* **2006**, *18*, 2073–2094.
- (45) Xia, Y. D.; Yang, Z. X.; Mokaya, R. Templated Nanoscale Porous Carbons. *Nanoscale* **2010**, *2*, 639–659.
- (46) Sakintuna, B.; Yurum, Y. Templated Porous Carbons: A Review Article. *Ind. Eng. Chem. Res.* **2005**, *44*, 2893–2902.
- (47) Park, S.-H. K.; Hwang, C.-S.; Ryu, M.; Yang, S.; Byun, C.; Shin, J.; Lee, J.-I.; Lee, K.; Oh, M. S.; Im, S. Transparent and Photo-Stable Zno Thin-Film Transistors to Drive an Active Matrix Organic-Light-Emitting-Diode Display Panel. *Adv. Mater.* **2009**, *21*, *678*–*682*.
- (48) Zhou, F.; Li, Z.; Shenoy, G. J.; Li, L.; Liu, H. Enhanced Room-Temperature Corrosion of Copper in the Presence of Graphene. *ACS Nano* **2013**, *7*, 6939–6947.
- (49) Tuinstra, F.; Koenig, J. L. Raman Spectrum of Graphite. *J. Chem. Phys.* **1970**, *53*, 1126–1130.
- (50) Cançado, L. G.; Takai, K.; Enoki, T.; Endo, M.; Kim, Y. A.; Mizusaki, H.; Jorio, A.; Coelho, L. N.; Magalhães-Paniago, R.; Pimenta, M. A. General Equation for the Determination of the Crystallite Size La of Nanographite by Raman Spectroscopy. *Appl. Phys. Lett.* **2006**, *88*, 163106.
- (51) Lucchese, M. M.; Stavale, F.; Ferreira, E. H. M.; Vilani, C.; Moutinho, M. V. O.; Capaz, R. B.; Achete, C. A.; Jorio, A. Quantifying Ion-Induced Defects and Raman Relaxation Length in Graphene. *Carbon* **2010**, *48*, 1592–1597.
- (52) Ke, Y.; Ong, L. L.; Sun, W.; Song, J.; Dong, M.; Shih, W. M.; Yin, P. DNA Brick Crystals with Prescribed Depths. *Nat. Chem.* **2014**, *6*, 994–1002.

(53) Yu, J.-S.; Yoon, S. B.; Chai, G. S. Ordered Uniform Porous Carbon by Carbonization of Sugars. *Carbon* **2001**, *39*, 1442–1446.

- (54) Nemes-Incze, P.; Osváth, Z.; Kamarás, K.; Biró, L. P. Anomalies in Thickness Measurements of Graphene and Few Layer Graphite Crystals by Tapping Mode Atomic Force Microscopy. *Carbon* **2008**, 46, 1435–1442.
- (55) Kaburagi, Y.; Hishiyama, Y. Highly Crystallized Graphite Films Prepared by High-Temperature Heat-Treatment from Carbonized Aromatic Polyimide Films. *Carbon* **1995**, 33, 773–777.
- (56) Hishiyama, Y.; Yoshida, A.; Kaburagi, Y.; Inagaki, M. Graphite Films Prepared from Carbonized Polyimide Films. *Carbon* **1992**, *30*, 333–337.
- (57) Sokolov, A. N.; Yap, F. L.; Liu, N.; Kim, K.; Ci, L. J.; Johnson, O. B.; Wang, H. L.; Vosgueritchian, M.; Koh, A. L.; Chen, J. H.; Park, J.; Bao, Z. N. Direct Growth of Aligned Graphitic Nanoribbons from a DNA Template by Chemical Vapour Deposition. *Nat. Commun.* **2013**, 4, 2402
- (58) Li, Z.; Wang, Y.; Kozbial, A.; Shenoy, G.; Zhou, F.; McGinley, R.; Ireland, P.; Morganstein, B.; Kunkel, A.; Surwade, S. P.; Li, L.; Liu, H. Effect of Airborne Contaminants on the Wettability of Supported Graphene and Graphite. *Nat. Mater.* **2013**, *12*, 925–931.
- (59) Heyman, A.; Musgrave, C. B. A Quantum Chemical Study of the Atomic Layer Deposition of Al2o3 Using Alcl3 and H2o as Precursors. *J. Phys. Chem. B* **2004**, *108*, 5718–5725.